

# Interference in Poisson Networks with Isotropically Distributed Nodes

Ralph Tanbourgi, *Student Member, IEEE*, Holger Jäkel, *Member, IEEE* and

Friedrich K. Jondral, *Senior Member, IEEE*

## Abstract

Practical wireless networks are finite, and hence non-stationary with nodes typically non-homogeneously deployed over the area. This leads to a location-dependent performance and to boundary effects which are both often neglected in network modeling. In this work, interference in networks with nodes distributed according to an isotropic but not necessarily stationary Poisson point process (PPP) are studied. The resulting link performance is precisely characterized as a function of (i) an arbitrary receiver location and of (ii) an arbitrary isotropic shape of the spatial distribution. Closed-form expressions for the first moment and the Laplace transform of the interference are derived for the path loss exponents  $\alpha = 2$  and  $\alpha = 4$ , and simple bounds are derived for other cases. The developed model is applied to practical problems in network analysis: for instance, the accuracy loss due to neglecting border effects is shown to be undesirably high within transition regions of certain deployment scenarios. Using a throughput metric not relying on the stationarity of the spatial node distribution, the spatial throughput locally around a given node is characterized.

## Index Terms

Wireless networks, non-stationary Poisson point process, interference, boundary effects, local throughput

The authors are with the Communications Engineering Lab, Karlsruhe Institute of Technology, Germany. Email: {ralph.tanbourgi, holger.jaekel, friedrich.jondral}@kit.edu. The authors gratefully acknowledge that their work is partially supported within the Priority Program 1397 "COIN" under grant No. JO 258/21-1 by the German Research Foundation (DFG). This work was presented in part at IEEE Int. Symposium on Inf. Theory, MA, USA, July 2012.

## I. INTRODUCTION

*Stochastic geometry*, in particular the theory of point processes, has recently attracted much attention in the field of interference modeling and performance analysis for wireless networks with many uncertainties such as mobile/dynamic user locations and channel fading. In a nutshell, the locations of the nodes are modeled as a realization of a stochastic point process rather than assuming a fixed spatial configuration. Since the emitted signals undergo a distant-dependent path loss, the interference experienced by a given node becomes random. Its statistical properties, moreover, depend on several factors including the law of the *spatial distribution* of nodes.

### A. Related Work and Motivation

Interference modeling and network analysis using tools from stochastic geometry have become a multi-faceted research field [1]–[20]. Early works on interference modeling assumed a stationary PPP for the interferer locations, cf. [1], [2]. Using a similar model, the spatial throughput of decentralized networks with Aloha medium access control (MAC) was analyzed in [3], [4]. Following these works, the node locations have mostly been modeled by *stationary* point processes which typically leads to *location-independent* statistical properties of the considered performance quantities, e.g., interference, outage probability or throughput. Among these advances, the transmission capacity framework [5]–[9] substantially contributed to a better understanding of the interactions between the basic system parameters of a wireless network. Besides, stationary models with *non-homogeneous* node deployments, e.g., Poisson-Cluster [10] and Matérn hard-core models [11], [12], were also investigated as such models are well-suited for studying more sophisticated medium access control (MAC) schemes. Treated as *general motion-invariant*, these models were further analyzed in [13]–[15] in a unifying way.

Stationarity of the spatial distribution of nodes is a desirable property since it allows for analytic tractability and, even more important, it represents a key requirement for applying certain performance metrics such as the transmission capacity metric [5]. In practice though, wireless networks exhibit a non-stationary spatial node distribution; for instance, because of a finite network area with boundary regions. Consequently, performance-relevant quantities such as the

experienced interference typically vary across the network area, thereby complicating modeling and system design. Besides this simple example, more complex deployments are often found in practice, e.g., wireless sensor networks created by airdrop [21] or spontaneous formation of hot spots [22]. The spatial configuration of such hotspots is typically dictated by user motion and by geometric constraints as illustrated in [23] for the example of a campus-wide Wi-Fi deployment. Furthermore, there is a growing need for cellular operators to better understand not only the temporal variations in user traffic demands but also its spatial dependence; for instance, the optimal interplay between small-cell deployments and Wi-Fi offloading—a promising approach to boost capacity in dense areas—requires carefully pinpointing areas of peak-traffic demands [24] and identifying locations for deployment so to reach the mobile users [25]. Hence, analytic tools for quantifying the network performance while taking into account user mobility as well as hard-to-predict spatial configurations are of eminent importance.

The need for non-stationary models for characterizing more complex node deployments was reported for instance in [26]. The authors discussed techniques that generate non-uniform node distributions for the purpose of efficient network simulations. In [16], a non-stationary and isotropic node distribution was assumed for analyzing multi-antenna receivers in the presence of interference. The analysis showed that the shape of the spatial distribution has a considerable impact on link performance. In [27], a first attempt was made towards analyzing the link performance at an arbitrary receiver location and for an arbitrary isotropic node distribution.

The shortcomings associated with the stationarity assumption are summarized below:

*Infiniteness and boundary effects:* Stationarity implies that the network consists of infinitely many nodes spread over an infinitely large region. However, the number of nodes as well as the network area is finite in practice. Boundary effects are ignored although they play a critical role in real-world networks because of unequal performance among the nodes in terms of, e.g., local topology, interference-/noise-limited performance, etc. Ensuring the quality-of-service (QoS) level targeted before deployment hence becomes difficult.

*Model artifacts for path loss exponent  $\alpha = 2$ :* In the stationary case and with a path loss exponent of  $\alpha = 2$ , the sum interference is almost surely (a.s.) infinite [5]. More specifically,

stationary models lose their accuracy as the path loss exponent  $\alpha$  tends to 2 since interference then becomes dominated by the infinite number of far nodes.

*Lack of local throughput metric:* Non-stationary models prevent the use of certain throughput metrics such as the transmission capacity. This is because it is no longer possible to infer the global performance from the local analysis as the local performance is location-dependent in non-stationary deployments.

### B. Contributions and Outcomes

We extend prior work by modeling the node locations by an *isotropic* PPP, with stationarity being a special case. The network model is explained in detail in Section II. The contributions are summarized below.

*Interference characterization:* The first moment and distribution function are studied for both arbitrary and Rayleigh fading channels. In the case of arbitrary fading, we derive in closed-form the exact first moment as a function of the spatial shape of the node distribution and of the arbitrary receiver location for the path loss exponents  $\alpha = 2$  and  $\alpha = 4$  in Section III-A. Using these results, an upper bound on the tail probability of the interference is derived. A corresponding lower bound that is not limited to the above values of  $\alpha$  is also presented for suitable spatial shapes. In Section III-B, we derive the Laplace transform of the interference for the Rayleigh fading model. We also address the case  $\alpha = 2$ , which eluded a meaningful analysis in the stationary model. One important insight is that for  $\alpha = 2$ , one can find situations in which a.s. infinitely many nodes contribute to the interference while the interference remains finite a.s. This result sharpens prior statements about the nature of the interference for  $\alpha = 2$  and suggests that there exists a transition between sparse and dense networks.

*Outage probability and model accuracy:* The location-dependent outage probability is characterized in Section IV-A as a function of the spatial shape. We demonstrate the use of the developed model in Section IV-B by comparing it to a stationary model that uses a local approximation capturing the non-homogeneity in the spatial nodes distribution. We show that, depending on the spatial shape in question, large approximation errors are avoided by the developed model,

particularly in transition areas where boundary effects come into play.

*Applications:* We propose a metric that is capable of quantifying the local throughput in non-stationary networks in Section V and demonstrate through an example how this metric can be used. In this example, we refine an existing result on code division multiple access (CDMA) systems in decentralized networks for the case  $\alpha = 2$ . We also show how the model accuracy for carrier-sense based MACs in decentralized networks can be significantly increased by means of the developed model.

**Notation:** Sans-serif-style letters ( $z$ ) represent random variables while serif-style letters ( $z$ ) represent deterministic variables or constants. The imaginary unit is given by  $j = \sqrt{-1}$  and  $\Re(\cdot)$  denotes the real part of a complex-valued number. We define by  $b(z, r)$  and  $\partial b(z, r)$  a disc and a circle, respectively, centered at  $z \in \mathbb{R}^2$  with radius  $r > 0$ . The origin is denoted by  $o$ .

## II. MATHEMATICAL MODEL

We consider a packet-based wireless network with identically-equipped nodes isotropically distributed in  $\mathbb{R}^2$ . The nodes are assumed to be slot-synchronized. In a randomly chosen slot, some nodes wish to transmit a packet. We assume that the locations  $x_1, x_2, \dots$  of these transmitters follow an isotropic PPP  $\Phi \triangleq \{x_i\}_{i=1}^\infty$  on  $\mathbb{R}^2$  with intensity (equivalently, density)  $\lambda(x)$  being defined on  $\mathbb{R}^2$ . Throughout this work we will denote by  $x_i$  to the random location of the  $i$ -th node as well as to the  $i$ -th node itself. Due to isotropy of  $\Phi$ ,  $\lambda(x)$  is rotation-invariant [28] and depends solely on the distance  $\|x\|$  to the origin, i.e.,  $\lambda(x) = \lambda(\|x\|e^{j\theta})$  for all  $\theta \in [-\pi, \pi)$ .<sup>1</sup> For notational convenience, we define  $r \triangleq \|x\|$ . The next definition is a consequence of the fact that  $\lambda(x)$  can be described as the resulting intensity after *location-dependent* thinning of a stationary PPP of some constant intensity [11].

**Definition 1.** *The shape function  $F : \mathbb{R}_{\geq 0} \mapsto [0, 1]$ , reflecting the spatial shape of  $\Phi$ , is defined on by the relation  $\lambda(x) = \lambda F(\|x\|)$ , where  $0 < \lambda < \infty$  is some intensity scaling constant.*

<sup>1</sup>In a very few situations, we will switch between Cartesian coordinates ( $x$ ) and the corresponding polar coordinates ( $\|x\|e^{j\theta}$ ) when appropriate. We do not expect any confusion thereof.

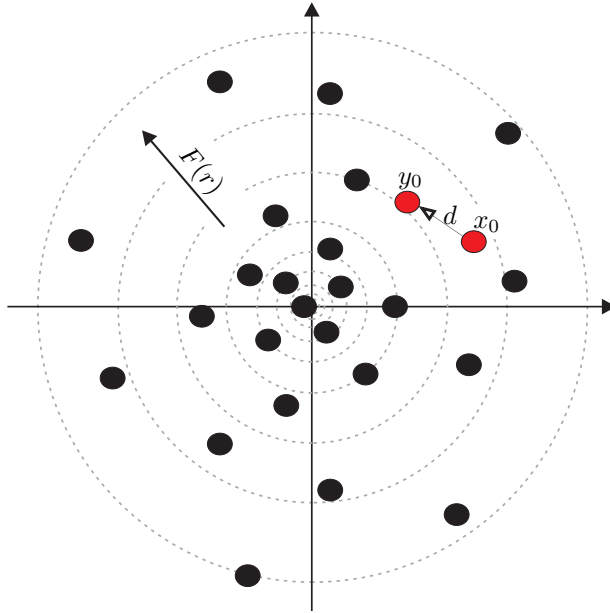


Fig. 1. System model: The reference receiver is located at  $y_0$  with distance  $\|y_0\|$  to the origin. The associated reference transmitter is located  $d$  units away from  $y_0$  at location  $x_0$ . Black dots represent interferers with random locations  $x_1, x_2, \dots$ . Shape function  $F(r)$  characterizes density of interferer set  $\Phi$  over distance  $r$  to the origin.

We assume that each transmitter  $x_i$  has an intended receiver located at fixed distance  $d$ . The fixed distance assumption, which can be seen as a *target* transmission distance dictated by the network protocol, is commonly accepted, see for example [5]. In order to measure the (spatially-averaged) link performance in the network we define a *reference link*, cf. [7]; the reference link consists of a reference receiver placed at an *arbitrary* location  $y_0 \in \mathbb{R}^2$  and of an associated reference transmitter placed at  $x_0$ , where  $x_0$  lies somewhere on the circle  $\partial b(y_0, d)$ . Note that neither the receiver  $y_0$  nor the transmitter  $x_0$  are part of the point process  $\Phi$ . By the Slivnyak-Mecke Theorem [28], the statistics of  $\Phi$  are not affected by the addition of the reference link.

We consider a path loss plus block-fading channel with independent and identically distributed (i.i.d.) fading coefficients. The power path loss between two locations  $x, y \in \mathbb{R}^2$  is given by the path loss function  $\ell(\|x - y\|) \triangleq (c + \|x - y\|^\alpha)^{-1}$  with path loss exponent  $\alpha \geq 2$ , where  $c \geq 0$  ensures boundedness of  $\ell$ . The power fading coefficient between a transmitter at  $x$  and the reference receiver  $y_0$  is given by  $g_x$ , where  $\mathbb{E}[g_x] = 1$  for all  $x$ . When appropriate we will drop the index  $x$  in  $g_x$ .

We assume that all nodes transmit with the same fixed transmit power and at a common information rate. The sum interference power at the reference receiver  $y_0$  is then given by

$$I(y_0) \triangleq \sum_{x \in \Phi} g_x \ell(\|x - y_0\|). \quad (1)$$

Treating interference as white noise, the instantaneous signal-to-interference-plus-noise ratio SINR at the reference receiver  $y_0$  is given by

$$\text{SINR}(y_0) \triangleq \frac{g_{x_0}}{\frac{1}{\eta} + \ell(d)^{-1} I(y_0)}, \quad (2)$$

where  $\eta$  is the average signal-to-noise ratio. We assume that the nodes employ strong channel coding such that the outage event is a steep function of the SINR. Focusing on the case where explicit transmitter coordination as well as CSI feedback is not possible, the outage probability is a useful metric for characterizing the link performance.

**Definition 2.** *The outage probability of the reference link  $x_0 \rightarrow y_0$  is given by*

$$P_o(y_0) \triangleq \mathbb{P}(\text{SINR}(y_0) < \beta), \quad (3)$$

where  $\beta$  is a modulation and coding specific threshold.

#### A. Spatial shapes chosen for illustrations

We next introduce four exemplary spatial shapes used for illustrations and numerical evaluations. They are chosen such to roughly characterize typical scenarios in wireless networks and to help increasing the reader's intuition about the results. An exact validation of the chosen spatial models through comparison with real-world deployments is outside the scope of this paper. The spatial shapes are depicted in Fig. 2.

- *Scenario a), finite network:* This scenario reflects the basic property all practical networks share: the network area is finite, or equivalently, the node density tends to zero for sufficiently large distances to the network center. It is assumed that the density first remains constant over a wide range as in the stationary case. At the network boundary the density then starts

to decay rapidly until it becomes zero.

- *Scenario b), urban with hotspot:* In urban scenarios there may sometimes exist small areas with very high data traffic, i.e., communications hotspots. They are typically found in commercial areas or other public places, comprising many densely—and sometimes dynamically—deployed wireless architectures [29]. We model such a hotspot scenario by “adding a plateau of density” around the origin on top of an already existing level of density corresponding to the urban deployment. This level then decays to zero with increasing distance to the origin to reflect finiteness of the network.
- *Scenario c), scattered decentralized network:* There are certain types of applications that preclude a detailed network layout for the reason of hostile environments or limited geographic access. For instance, large sensor networks are sometimes created by airdrop which results in a highly scattered spatial distribution of devices. We model such a behavior by an exponentially decreasing density around the origin.
- *Scenario d), carrier sensing in decentralized networks:* This scenario is found in decentralized networks with transmitters employing carrier sensing to avoid excessive interference; suppose a transmitter (here located in the origin) is granted access to the medium. Consequently, other potential transmitters directly surrounding this transmitter defer their transmission as they sense the medium as busy, while other potential transmitters farther away sense the medium as free and therefore start to transmit, cf. Section V-B for more details.

### III. INTERFERENCE ANALYSIS

We now study the interference statistics at the reference receiver  $y_0$ . The analysis first focuses on the case of an arbitrary fading distribution. We derive the first moment of the interference and then use bounding techniques such as those used in [5] to characterize the interference distribution. For the Rayleigh model, we then derive the Laplace transform of the interference distribution.



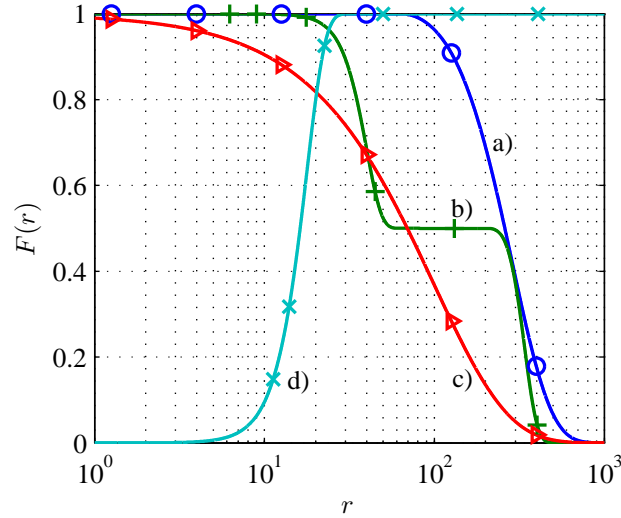


Fig. 2. The four exemplary spatial shapes considered in this work. Scenario a) (finite network), Scenario b) (urban with hotspot), Scenario c) (scattered decentralized network) and Scenario d) (carrier sensing in decentralized networks).

### A. Arbitrary Fading Model

1) *First Moment of the Interference*: The first moment of the interference  $\mathbb{E}[I(y_0)]$  measured at the reference receiver  $y_0$  can in general be obtained by

$$\int_0^{\infty} \mathbb{P}(I(y_0) \geq z) dz. \quad (4)$$

Obviously, one would have to know the distribution of  $I(y_0)$ , which unfortunately is known in closed-form only for a few cases of stationary point processes [13]. A remedy to this problem is given by the Campbell Theorem [28], which allows us to derive the first result:

**Theorem 1.** *Let  $f(r) \triangleq dF(r)/dr$ ,  $c > 0$ ,  $\alpha = 2$  and  $\|y_0\| > 0$ . If  $F(r) \stackrel{r \rightarrow \infty}{\sim} \frac{1}{r^\nu}$  for some  $\nu > 0$ , then*

$$\mathbb{E}[I(y_0)] = \lambda A_2(y_0, c) < \infty, \quad (5)$$

where  $A_2(y_0, c)$  is given by

$$A_2(y_0, c) = -\pi \left( F(0) \operatorname{asinh} \frac{c - \|y_0\|^2}{2\|y_0\|\sqrt{c}} + \int_0^{\infty} f(r) \operatorname{asinh} \frac{r^2 + c - \|y_0\|^2}{2\|y_0\|\sqrt{c}} dr \right). \quad (6)$$

A proof is given in Appendix B. The condition  $F(r) \stackrel{r \rightarrow \infty}{\sim} \frac{1}{r^\nu}$  for some  $\nu > 0$  is necessary for  $\mathbb{E}[I(y_0)]$  to exist. The function  $A_2(y_0, c)$  in (6) has an interesting interpretation: it can be seen as the *interference-driving* function as it determines the interference up to a scaling factor. Additionally, the first term in (6) can be interpreted as the interference field associated with the origin  $o$ , while the second term effectively adds up the interference according to  $f(r)$ .

**Remark 1.** *If the reference receiver is located in the origin ( $\|y_0\| = 0$ ), the asinh-term in  $A_2(y_0, c)$  has to be replaced by  $\log(r^2 + \|y_0\|^2 + c)$ , cf. Identity 2 in Appendix A.*

Glancing at the second term in (6), we note:

**Corollary 1.** *When  $F(0) = 1$  and  $f(r) \leq 0$  for all  $r \in \mathbb{R}_+$ ,  $F(r)$  can be interpreted as a complementary cumulative distribution function (CDF) with respect to a random distance  $r$  to the origin, yielding*

$$A_2(y_0, c) = -\pi \operatorname{asinh} \frac{c - \|y_0\|^2}{2\|y_0\|\sqrt{c}} + \pi \mathbb{E} \left[ \operatorname{asinh} \frac{r^2 + c - \|y_0\|^2}{2\|y_0\|\sqrt{c}} \right]. \quad (7)$$

Corollary 1 states that the integral in (6) can be seen as an *averaging* of the interference with respect to a random distance  $r$ . Such a representation may be appropriate when analyzing networks with *a priori* unknown or fast-varying spatial configurations, for which a CDF is then used to model their spatial shape.

**Corollary 2.** *Let  $F(r) \stackrel{r \rightarrow \infty}{\sim} \frac{1}{r^\nu}$  for some  $\nu \in (0, 2]$ . Then, the expected number of interferers  $\mathbb{E}[|\Phi|] = 2\pi\lambda \int_0^\infty rF(r) dr = \infty$  but the expected interference  $\mathbb{E}[I(y_0)] < \infty$ .*

The intuition behind Corollary 2 is that, although the expected number of nodes contributing to the interference is unbounded, the network remains sufficiently sparse such that the first moment of the interference remains bounded. Note that for a PPP, if the expected number of interferers is unbounded, this implies that the number of interferers is a.s. infinite which can be verified by studying the Laplace transform of the PPP [28], [30]. Applying the Markov Inequality  $\mathbb{P}(z \geq z) \leq \frac{1}{z} \mathbb{E}[z]$  [31], this in turn means that the number of nodes is a.s. infinite while the

interference remains a.s. finite. This particular finding is somewhat remarkable since it rearranges the commonly-accepted perception, stating that whenever  $\alpha = 2$  and the number of interferers is a.s. infinite, the interference is a.s. infinite as well [7], [13]. This perception indeed holds for stationary point processes but does not hold in general for non-stationary point processes, as demonstrated by Corollary 2.

**Theorem 2.** *Let  $F(r) \stackrel{r \rightarrow \infty}{\sim} \frac{1}{r^\nu}$  for  $\nu \rightarrow 0$ . Then,  $I(y_0) = \infty$  a.s.*

A proof is given in Appendix B. Theorem 2 shows that whenever  $F(r)$  decays at most logarithmically, the interference is a.s. infinite. In particular, this includes the stationary case (since  $\lim_{r \rightarrow \infty} F(r) > 0$ ) which is consistent with the literature [13]. Combining Corollary 2 and Theorem 2, we observe that for asymptotically decaying  $F(r)$  there exists a transition between *sparse* and *dense* networks. This transition determines whether or not the interference is a.s. finite in a non-stationary Poisson network with a.s. infinite number of interferers.

**Remark 2.** *By setting  $g \equiv 1$ , the pure path loss case is also covered by the above results.*

We now characterize the first moment of the interference for the case  $\alpha = 4$ .

**Theorem 3.** *Let  $f(r) \triangleq dF(r)/dr$ ,  $c > 0$  and  $\alpha = 4$ . Then,*

$$\mathbb{E}[I(y_0)] = \lambda A_4(y_0, c) < \infty, \quad (8)$$

where  $A_4(y_0, c)$  is given by

$$A_4(y_0, c) = \frac{\pi}{2\sqrt{c}} \left( F(r) \arctan \frac{2\Re\{\kappa(r, c, y_0)\}}{1 - |\kappa(r, c, y_0)|^2} \Big|_{r=0}^{\infty} - \int_0^{\infty} f(r) \arctan \frac{2\Re\{\kappa(r, c, y_0)\}}{1 - |\kappa(r, c, y_0)|^2} dr \right) \quad (9)$$

and  $\kappa(r, c, y_0)$  is given by (27) in Appendix A.

A proof is given in Appendix B. The term  $A_4(y_0, c)$  in (9) can be again interpreted as the interference-driving function.

**Corollary 3.** *Let  $F(r) = 1$  so that  $f(r) = 0$  (stationary PPP). Then, by carefully taking the*

limits

$$\lim_{r \rightarrow a} \arctan \frac{2\Re\{\kappa(r, c, y_0)\}}{1 - |\kappa(r, c, y_0)|^2} = \begin{cases} -\frac{\pi}{2}, & a = 0 \\ \frac{\pi}{2}, & a = \infty, \end{cases}$$

the well-known result  $\mathbb{E}[I(y_0)] = \lambda \frac{\pi^2}{2\sqrt{c}}$  for the stationary PPP is recovered [13].

2) *Bounds on the Interference Distribution:* We next treat the problem of bounding the tail of  $\mathbb{P}(I(y_0) \geq z)$ . A simple upper bound can be obtained using Markov's inequality in combination with Theorem 1 and Theorem 3. For the construction of a lower bound, we first recall the definition of subharmonic functions.

**Definition 3.** (Subharmonic functions [32, Ch. 2]): Let  $G \subseteq \mathbb{R}^n$  be an open set and let  $h(x)$  be a function twice continuously differentiable on  $G$ . If  $\sum_{k=1}^n \frac{\partial^2}{\partial x_k^2} h(x) \geq 0$  on  $G$ , then  $h(x)$  is called subharmonic on  $G$ .

If  $F(r)$  is convex in a certain (one-dimensional) region, then the intensity  $\lambda(x)$  is subharmonic on the corresponding (two-dimensional) region. Such a behavior may be often found at the network boundary, e.g., Scenario a) and b), or when the shape function exhibits a tail, e.g., Scenario c) and d). In this case a lower bound on the tail probability  $\mathbb{P}(I(y_0) \geq z)$  can be derived:

**Theorem 4.** Let  $\lambda(x)$  be subharmonic on  $G \subseteq \mathbb{R}^2$  and let  $y_0 \in G$ . Denote by  $\bar{r}(x)$  the maximum radius for which the closed ball  $b(x, t)$  is contained in  $G$ , i.e.,  $\bar{r}(x) = \max\{t \in \mathbb{R}_+ : b(x, t) \subseteq G\}$ .

Then,

$$\mathbb{P}(I(y_0) \geq z) \geq 1 - \exp\left(-2\pi\lambda F(\|y_0\|) \int_0^{\bar{r}(y_0)} r \mathbb{P}(\mathbf{g} \geq z(c + r^\alpha)) dr\right). \quad (10)$$

A proof is given in Appendix B. Note that subharmonicity includes the case of harmonicity. The construction of the lower bound in Theorem 4 basically builds on the so-called ‘‘dominant interferer’’ phenomenon introduced in [7], where it was also reported that the resulting bound is fairly tight. However, in our case the tightness of (10) strongly depends on the second derivative

of  $F(r)$  and may not be guaranteed.

**Corollary 4.** *Let  $z < \frac{1}{c}$ . For the pure path loss model ( $g \equiv 1$ ), (10) reduces to*

$$\mathbb{P}(I(y_0) \geq z) \geq 1 - \exp\left(-\pi\lambda F(\|y_0\|) \min\left\{\bar{r}^2(y_0), \left(\frac{1}{z} - c\right)^{\frac{2}{\alpha}}\right\}\right). \quad (11)$$

The restriction  $z < \frac{1}{c}$  is necessary to allow the closest interferer to be dominant, otherwise this bounding technique would yield the trivial lower bound  $\mathbb{P}(I(y_0) \geq z) \geq 0$ .

Using the Markov Inequality [31], we obtain the simple upper bound

$$\mathbb{P}(I(y_0) \geq z) \leq \frac{\lambda}{z} A_\alpha(y_0, c), \quad (12)$$

for the cases  $\alpha = 2$  and  $\alpha = 4$ , where  $A_2(y_0, c)$  and  $A_4(y_0, c)$  are given by (6) and (9), respectively.

### B. Rayleigh Fading Model

For the commonly-used Rayleigh fading model, it was demonstrated in [4] that the Laplace transform of the interference is useful for computing outage probabilities. We therefore derive the Laplace transform of  $I(y_0)$ , i.e.,  $\mathcal{L}_{I(y_0)}(s) = \mathbb{E}[e^{-sI(y_0)}]$  next for arbitrary  $y_0$  and  $F(r)$ . Similar to Section III-A, we focus again on  $\alpha = 2$  and  $\alpha = 4$ .

**Theorem 5.** *In the Rayleigh fading model, the Laplace transform of  $I(y_0)$  at  $y_0$  is given by*

$$\mathcal{L}_{I(y_0)}(s) = \exp(-\lambda s A_\alpha(y_0, s + c)), \quad (13)$$

for the cases  $\alpha = 2$  and  $\alpha = 4$ , where  $A_2(y_0, c)$  and  $A_4(y_0, c)$  are given by (6) and (9), respectively.

A proof is given in Appendix B. Note that for  $\alpha = 2$  and  $F(r) \stackrel{r \rightarrow \infty}{\sim} \frac{1}{r^\nu}$  for every  $\nu \rightarrow 0$ , we have that  $\mathcal{L}_{I(y_0)}(s) = 0$  for all  $s$ . This in turn implies  $I(y_0) = \infty$  a.s. which is consistent with Theorem 2.

**Remark 3.** *Setting  $F(r) = 1$  for all  $r \in \mathbb{R}_+$  and  $c = 0$ , we recover the well-known result for*

the homogeneous case with  $\alpha = 4$ :  $\mathcal{L}_{l(y_0)}(s) = \exp(-\lambda \frac{\pi^2}{2} \sqrt{s})$ .

**Remark 4.** *The case  $\alpha = 2$  with Rayleigh fading may seem contradictory first: A path loss exponent equal to  $\alpha = 2$  is typically observed in propagation environments without ground-plane reflection [33]. In contrast, Rayleigh fading models the non-line-of-sight (NLOS) case with many reflected paths impinging at the receiver. It turns out, however, that there may truly exist urban NLOS scenarios with considerably small path loss exponents ( $\alpha \sim 2.6$ ) as demonstrated in [34]. Depending on the geometry of objects in the proximity of the receiver, the received signal may therefore still undergo severe small-scale fading. Hence, the case  $\alpha = 2$  may serve as a theoretical limit of what can be expected roughly in Rayleigh fading environments with a small path loss exponent.*

#### IV. OUTAGE PROBABILITY AND MODEL ACCURACY

In this section, the outage probability is characterized for the underlying setting and the model accuracy is studied.

##### A. Outage Probability

For arbitrary fading the bounds on the tail probability of  $l(y_0)$  can be used to bound the outage probability, see for example [7]. In the sequel, we will focus on the Rayleigh fading case and discuss the impact of the spatial shape on the resulting performance.

**Corollary 5.** *The outage probability  $P_o(y_0)$  at  $y_0$  in the Rayleigh fading model is*

$$P_o(y_0) = 1 - \mathcal{L}_{l(y_0)}(\beta(c + d^\alpha)) e^{-\frac{\beta}{\eta}}, \quad (14)$$

for the cases  $\alpha = 2$  and  $\alpha = 4$ , where  $\mathcal{L}_{l(y_0)}$  is given by (13).

Corollary 5 now allows for measuring the exact outage probability at an arbitrary location  $y_0$  and for an arbitrary spatial shape function  $F(r)$ . Fig. 3 shows  $P_o(y_0)$  vs.  $\|y_0\|$  for  $\alpha = 2$  and  $\alpha = 4$ . The spatial shape function  $F(r)$  was chosen according to scenario a). In the noise-free case ( $\eta = \infty$ ) the outage probability decreases monotonically with increasing distance to

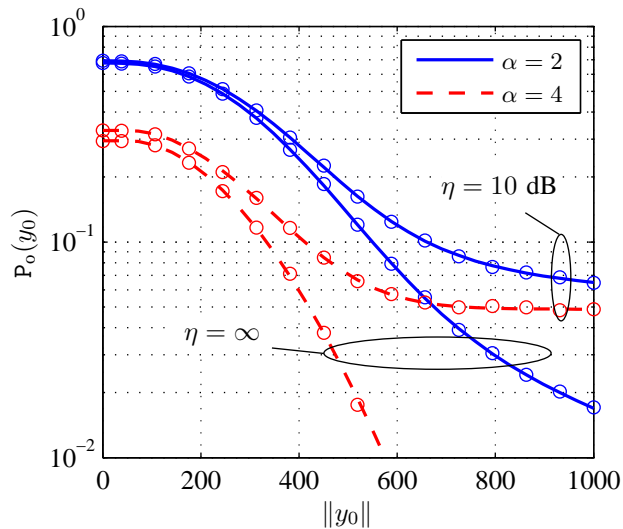


Fig. 3. Outage probability  $P_o(y_0)$  vs.  $\|y_0\|$ . Parameters were  $d = 10$ ,  $\beta = 0.5$ ,  $c = 1$ ,  $\lambda = 0.001$ . The spatial shape function  $F(r)$  was chosen according to scenario a). Marks represent simulation results.

the origin. Furthermore, we observe that for  $\alpha = 2$  the outage probability  $P_o(y_0)$  is higher and its slope is less steep than it is for  $\alpha = 4$ . This is because for  $\alpha = 2$  the individual interference contributions decay more slowly over distance than they do for  $\alpha = 4$ . As a result, the interference is no longer dominated by only a few nearby interferers but it is determined by the large number of nodes nodes, including those relatively far away from  $y_0$ . When receiver noise is considered ( $\eta = 10$  dB) the behavior of  $P_o(y_0)$  changes considerably: while  $P_o(y_0)$  is on the same order as in the noise-free case around the center of the network, both curves converge to a constant outage probability level as the reference receiver eaves the center of the network. In fact, in this boundary region outage is primarily due to bad fades rather than to interference, thus rendering the performance noise-limited rather than interference-limited. This transition—from the interference-limited to the noise-limited regime—can be precisely tracked owing to the developed model; for instance, Fig. 2 suggests that the noise-limited regime commences somewhere around  $\|y_0\| \approx 500$ , while Fig. 3 reveals that this is not true at least for  $\alpha = 2$  ( $\|y_0\| > 800$ ) for the reason explained above.

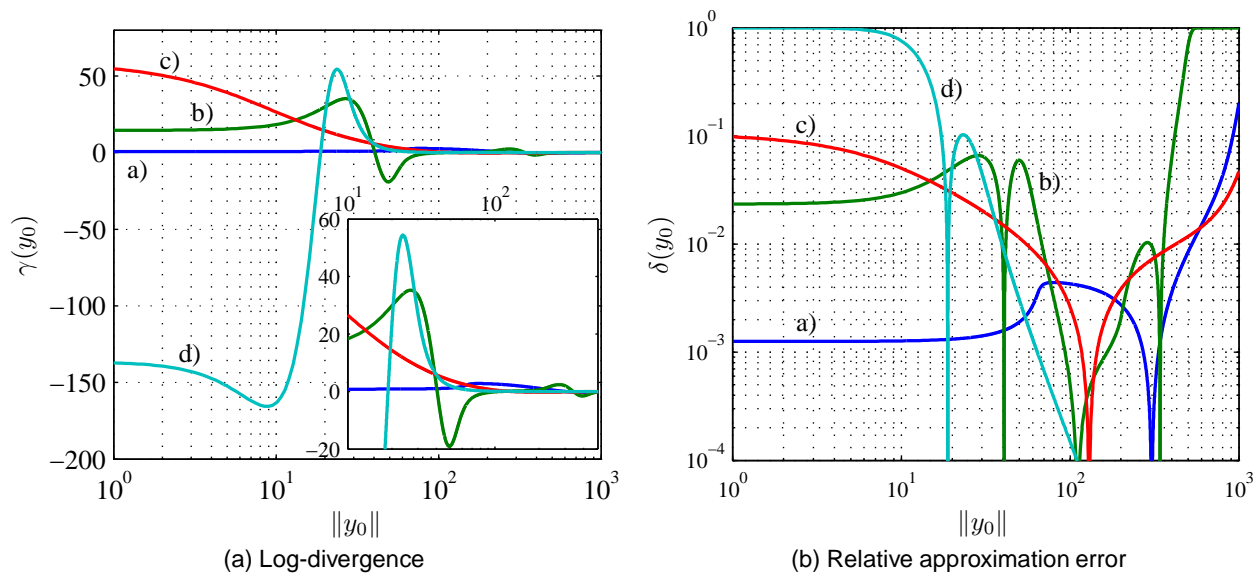


Fig. 4. (a) Log-divergence  $\gamma(y_0)$  vs.  $\|y_0\|$  for different shape functions. (b) Relative approximation error vs.  $\|y_0\|$  for different shape functions and  $\lambda = 10^{-3}$ . Parameters are  $\alpha = 4$ ,  $c = 0$ ,  $d = 10$  and  $\beta = 1$ .

### B. Exact vs. Approximate Model

Up to this point, it is not yet very clear how much can be gained by the interference model derived in this work. In order to quantify the gains, we compare our model to a simpler one that approximates the non-stationarity-property of the interference locally around the reference receiver  $y_0$ . In this simpler model, the interference field at  $y_0$  is assumed to originate from a stationary PPP having constant intensity  $\lambda F(\|y_0\|)$ ; in other words, the network-wide spatial distribution of interferers is approximated locally by the density at location  $y_0$ .

For the stationary case the outage probability for Rayleigh fading is well-known [3], [4]. With the above approximation the approximate outage probability  $\tilde{P}_o(y_0)$  at  $y_0$  is then given by

$$\tilde{P}_o(y_0) = 1 - \exp\left(-\lambda F(\|y_0\|) d^2 \beta_\alpha^{\frac{2}{\alpha}} \frac{2\pi^2}{\alpha} \csc \frac{2\pi}{\alpha}\right). \quad (15)$$

The intuition behind (15) is that the exact outage probability is approximated by taking the outage probability expression corresponding to the stationary case and modulating the intensity  $\lambda$  by the spatial shape function  $F(r)$  at  $r = \|y_0\|$ . To measure the difference between  $\tilde{P}_o(y_0)$  and  $P_o(y_0)$  we define the following metric.



**Definition 4** (Log-divergence). *The log-divergence is defined as*

$$\gamma(y_0) \triangleq \lambda^{-1} \log \frac{1 - P_o(y_0)}{1 - \tilde{P}_o(y_0)}. \quad (16)$$

The log-divergence  $\gamma(y_0)$  quantifies the ratio of the exact and approximate success probability  $(1 - P_o(y_0))$  on the logarithmic scale for arbitrary  $y_0$ . The normalization by  $\lambda$  is necessary to remove the dependency on  $\lambda$  so to measure the divergence resulting from the spatial shape only. For large positive  $\gamma(y_0)$  the approximation overestimates the true outage probability, while for large negative  $\gamma(y_0)$  outage probability is underestimated. The approximation is accurate whenever  $|\gamma(y_0)|$  is small. The log-divergence can be computed using Corollary 5.

**Corollary 6.** *In the Rayleigh fading model and for  $c = 0$ , the log-divergence for the case  $\alpha = 4$  is*

$$\gamma(y_0) = d^4 \beta \left( \frac{\pi^2 F(\|y_0\|)}{2d^2 \sqrt{\beta}} - A_4(y_0, \beta d^4) \right). \quad (17)$$

Fig. 4a shows the log-divergence  $\gamma(y_0)$  vs.  $\|y_0\|$  for the shape functions  $F(r)$  introduced in Section II-A. It can be seen that the log-divergence exhibits an oscillatory behavior that depends on the degree of variability of  $F(r)$ . For example,  $F(r)$  in scenario a) and c) changes comparably slow, and thus the corresponding log-divergence shows only weak oscillations. The log-divergence for scenario a) remains low ( $\gamma(y_0) \approx 0.80$ ) over a wide range which suggests that the local approximation works well in this case. As for scenario c), however, the log-divergence is large around the origin which is due to the fact that the outage probability is highly overestimated as the (exponential) decay of  $F(r)$  to the right-hand side is neglected by the approximation. A similar effect can be observed for scenario d): the outage probability is highly underestimated around the origin because the increasing density to the right-hand side is neglected. The log-divergence for scenario b) exhibits rich oscillations due to a stronger varying shape function. As can be seen, these oscillations are high particularly in the transition region ( $10^1 \leq r \leq 10^2$ ).

To understand the impact of the log-divergence on outage probability, the relative error

$$\delta(y_0) = \frac{|\tilde{P}_o(y_0) - P_o(y_0)|}{P_o(y_0)} \quad (18)$$

is shown in Fig. 4b for the example  $\lambda = 10^{-3}$ . Fig. 4b underlines the observations made in Fig. 4a: the approximation works well for scenario a) while for the other three scenarios the approximation is relatively loose. Especially for the scenarios b) and d), the relative error  $\delta(y_0)$  is considerably high over a wide range (between 1% and 10% around the network center for scenario c)). For scenario b) the relative error is approximately 10% around the density mid-level. In case of scenario d) the approximation completely fails around the origin.

## V. APPLICATIONS AND EXAMPLES

In this section, the developed model is applied to problems in network modeling with non-stationary spatial node distributions.

### A. Local Transmission Capacity

As argued in Section I, the transmission capacity metric cannot be applied to networks with non-stationary spatial node distributions. Based on the developed model, the definition of the transmission capacity can however be extended to account for non-stationarity and location dependency.

**Definition 5** (Local transmission capacity). *The local transmission capacity is defined as*

$$c(x, \epsilon) \triangleq \lambda(x, \epsilon)(1 - \epsilon), \quad (19)$$

*and gives the maximal density  $\lambda(x, \epsilon) \triangleq P_o^{-1}(x)$  of concurrent transmissions in an infinitesimal region around location  $x$  subject to an outage probability constraint  $\epsilon$ .*

Since the local transmission capacity accounts for the spatial shape, this metric allows throughput bottlenecks to be spatially tracked and properly engineered, e.g., by balancing QoS among nodes irrespective of their location. For isotropic node distributions, in particular, the local

transmission capacity depends on  $\|x\|$  and can be computed/bounded by algebraic manipulations of the outage probability expressions derived in the previous sections.

*Example: FH-CDMA vs. DS-CDMA in decentralized networks:* In [7] it was shown that in the stationary PPP model, the transmission capacity gain of frequency-hopping (FH)-CDMA compared to direct-sequence (DS)-CDMA scales as  $M^{1-\frac{2}{\alpha}}$ , where  $M$  is the processing gain. For very small path loss exponents ( $\alpha \rightarrow 2$ ) this result suggests that the gains of FH-CDMA vanish irrespective of the processing gain  $M$ . This observation, however, results from the stationarity assumption not being able to correctly capture the case  $\alpha = 2$ . The next result rearranges this scaling result for the case  $\alpha = 2$  for Rayleigh fading and the reference receiver located in the origin.

**Corollary 7.** *Let  $\alpha = 2$ ,  $c = 0$  and  $\eta = \infty$ . In the Rayleigh fading model, the local transmission capacity gain of FH-CDMA over DS-CDMA at  $o$  is*

$$\frac{c^{FH}(o, \epsilon)}{c^{DS}(o, \epsilon)} = 1 + \frac{F(0)}{A_2(o, \beta d^2)} \log M + O(1). \quad (20)$$

A proof is given in Appendix B. Surprisingly, this result shows that the gains of FH-CDMA over DS-CDMA do not vanish for  $\alpha = 2$  (as was predicted by [7]), but they scale with  $\log M$  which re-enforces the superiority of FH-CDMA over DS-CDMA in terms of transmission capacity.

### B. Interference in Networks with Transmitter-Inhibition

In order to study decentralized networks with inhibition mechanisms such as carrier-sense medium access (CSMA) or local frequency division multiple access (FDMA) while ensuring analytic tractability, methods based on non-homogeneous Poisson approximation have been proposed for stationary models [12], [18]–[20]. When such protocols are *transmitter-initiated*, e.g., transmitter sensing for CSMA, the resulting spatial distribution of interferers becomes non-homogeneous but remains isotropic around the inhibiting transmitter since potential transmitters around the inhibiting transmitter are kept silent while others located farther away are likely to

transmit. In contrast, the interference field at the associated receiver is not isotropic. To overcome this intractability, the receiver is assumed to be co-located with the inhibiting transmitter, thereby virtually rendering the interference field around the receiver isotropic at the cost of losing model accuracy. This loss depends on the distance between the inhibiting transmitter and the associated receiver. Using the developed model, we can now evaluate the accuracy loss resulting from assuming that transmitter and receiver are co-located for this CSMA modeling technique. We briefly summarize the basic ideas of this modeling technique and refer to [18], [19] for further details.

*Non-homogenous Poisson approximation for CSMA networks:* Let the potential interferers be initially distributed according to a stationary PPP of density  $\lambda$ . Assume that the reference transmitter  $x_0$  and the reference receiver are located at  $o$  and  $y_0$ , respectively, and separated by  $d$ . The inhibition mechanism is modeled in three steps: 1) The large-scale density of active interferers is derived using a Matérn-type 2 model [28], which captures the inhibition effect on a “macroscopic” level. The large-scale density  $\lambda_\ell$  is then given by

$$\lambda_\ell = \frac{1 - e^{-\lambda\pi\Gamma(1+\frac{2}{\alpha})\Delta^{-\frac{2}{\alpha}}}}{\pi\Gamma(1+\frac{2}{\alpha})\Delta^{-\frac{2}{\alpha}}}, \quad (21)$$

where  $\Delta > 0$  is the sensing threshold. We then condition on the fact that  $x_0$  is granted access to the channel and we are now seeking the statistical characterization of the interferers around  $x_0$  after this conditioning. 2) This is where the non-homogeneous Poisson approximation comes into play, yielding a “small-scale” density  $\lambda_s$

$$\lambda_s(r) = \lambda_\ell (1 - \exp(-\Delta r^\alpha)), \quad (22)$$

modeling the density of interferers around the reference transmitter  $x_0$ . The term  $1 - \exp(-\Delta r^\alpha)$  can be seen as the probability that an interferer at distance  $r$  to  $x_0$  does not sense the ongoing transmission of  $x_0$ . The behavior of  $\lambda_s(r)$  can be described by the spatial shape function of scenario d), cf. Fig. 2. 3) The density  $\lambda_s(r)$  in (22) is then used to describe the interference around the reference receiver  $y_0$ , although it reflects the interference experienced by the reference

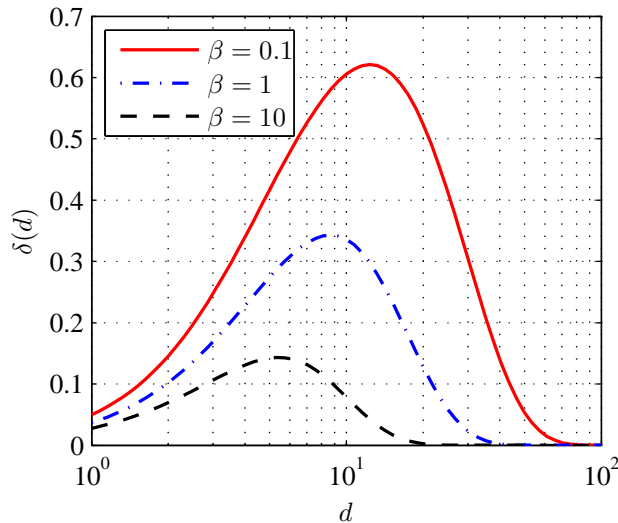


Fig. 5. (a) Relative accuracy loss  $\delta(d)$  vs. transmission distance  $d$  for different  $\beta$ . Parameters are  $\alpha = 4$ ,  $c = 0$ ,  $\lambda = 10^{-3}$  and  $\Delta = -50$  dB.

transmitter at  $x_0$ . This simplification step increases analytic tractability at the cost of losing accuracy. The level of accuracy loss resulting from step 3) is next studied for the Rayleigh fading model with  $\alpha = 4$  and  $c = 0$ . We use the same notion as in (18) to measure the relative accuracy loss as a function of  $d$ , i.e.,

$$\delta(d) \triangleq \frac{|\mathbb{P}_o(o, d) - \mathbb{P}_o(y_0, d)|}{\mathbb{P}_o(y_0, d)}, \quad \|y_0\| = d, \quad (23)$$

where the second argument in  $\mathbb{P}_o$  now highlights the dependence on  $d$ . Fig. 5 shows the accuracy loss vs.  $d$  for different  $\beta$  and  $\Delta = -50$  dB. The density of potential transmitters is  $\lambda = 10^{-3}$ . It can be seen that depending on the value of  $d$ , significant errors can occur. Interestingly, the relative accuracy loss decreases with  $\beta$  which is due to an increased outage correlation at the locations  $x_0$  and  $y_0$ . The error remains small for small  $d$ , i.e., short-range communications, for the same reason as above. For very large  $d$ ,  $\delta(d)$  tends to zero which results from both  $\mathbb{P}_o(o, d)$  and  $\mathbb{P}_o(y_0, d)$  tending to zero.

## VI. CONCLUSION

We extended prior work on interference modeling for wireless networks with isotropic but not necessarily stationary spatial distribution of nodes. The interference statistics and the outage probability were analyzed as a function of (i) an arbitrary receiver location inside the network and (ii) an arbitrary but isotropic node distribution. For the path loss exponents  $\alpha = 2$  and  $\alpha = 4$  closed-form expressions were obtained while bounds were derived for other cases. The developed model led to some interesting insights that could not have been revealed previously due to limiting the analysis to stationary models only. The usefulness of the results was discussed and demonstrated through examples in network analysis related to outage probability, local throughput characterization and carrier-sensing mechanisms. It was found that the developed model increases model accuracy significantly and provides an adequate tool to describe location-dependent performance in networks with practical node distribution.

### APPENDIX A

#### INTEGRAL IDENTITIES

**Identity 1.** *If  $a > |b|$ ,  $a, b \in \mathbb{R}$ , then*

$$\int_0^\pi \frac{d\phi}{(a + b \cos \phi)^{n+1}} = \frac{\pi P_n\left(\frac{a}{\sqrt{a^2 - b^2}}\right)}{(a^2 - b^2)^{\frac{n+1}{2}}}, \quad (24)$$

where  $P_n(x)$  is the  $n^{\text{th}}$ -Legendre polynomial [35]. We will be using  $n = 1$ , leading to the  $0^{\text{th}}$ -Legendre polynomial given by  $P_0(x) = 1$ .

**Identity 2.** *Let  $a_1, a_2, a_3 \in \mathbb{R}$ , where  $a_3 > 0$ . Define  $R \triangleq a_1 + a_2 t^2 + a_3 t^4$ ,  $T = 4a_1 a_3 - a_2^2$ . By [35] and using the substitution  $t \rightarrow t^2$ , we have*

$$\int \frac{2t\sqrt{a_3}}{\sqrt{a_1 + a_2 t^2 + a_3 t^4}} dt = \begin{cases} \log \frac{2\sqrt{a_3}R + 2a_3 t^2 + a_2}{\sqrt{T}}, & a_3 > 0 \\ \operatorname{asinh} \frac{2a_3 t^2 + a_2}{\sqrt{T}}, & T > 0 \\ \log(a_3 t^2 + \frac{a_2}{2}), & T = 0. \end{cases} \quad (25)$$

**Identity 3.** Let  $a_1, a_2 \in \mathbb{R}$ , where  $a_1 > 0$ . Then,

$$\int \int_0^\pi \frac{2t}{a_1 + (t^2 + a_2^2 - 2ta_2 \cos \phi)^2} d\phi dt = \frac{\pi}{2\sqrt{a_1}} \text{atan} \frac{2\Re\{\kappa(t, a_1, a_2)\}}{1 - |\kappa(t, a_1, a_2)|^2}, \quad (26)$$

where

$$\kappa(t, a_1, a_2) \triangleq \frac{t^2 - a_2^2 - j\sqrt{a_1}}{\sqrt{(\sqrt{a_1} + j(t^2 + a_2^2))^2 + 4t^2 a_2^2}}. \quad (27)$$

*Proof:* The basic idea is to decompose the integrand into partial fractions and to apply Identity 1 and 2, yielding (26) after some algebraic manipulations. Note that according to [35], (24) and (25) hold only for real-valued parameters. However, we verified that they also hold for complex-valued parameters.  $\square$

## APPENDIX B

### PROOFS

#### A. Proof of Theorem 1

We want to compute the expectation

$$\mathbb{E} \left[ \sum_{x \in \Phi} g_x \ell(\|x - y_0\|) \right], \quad (28)$$

where the expectation is with respect to the interferer locations and the channel gains  $g_x$ . Since the expectation operator linear, we can compute the expectation with respect to all  $g_x$  first, i.e.,  $\mathbb{E}[g_x] = 1 \forall x \in \Phi$ . Applying the Campbell Theorem, yields

$$\mathbb{E}[I(y_0)] = \lambda \int_{\mathbb{R}^2} \ell(\|x - y_0\|) F(\|x\|) dx. \quad (29)$$

Changing to polar coordinates and exploiting the isotropy property, we can rewrite (29) as

$$\mathbb{E}[I(y_0)] = \lambda \int_0^\infty \int_0^\pi \frac{2r F(r)}{c + (r^2 + \|y_0\|^2 - 2r\|y_0\| \cos \phi)} d\phi dr. \quad (30)$$

We then apply Identity 1 to the inner integral of (30) to obtain

$$\mathbb{E} [I(y_0)] = \lambda\pi \int_0^\infty \frac{2r F(r)}{\sqrt{(c + r^2 + \|y_0\|^2)^2 - 4r^2\|y_0\|^2}} dr. \quad (31)$$

Finally using product integration and applying Identity 2 to (31) and verifying the convergence of the upper limit using the constraint  $F(r) \stackrel{r \rightarrow \infty}{\sim} \frac{1}{r^\nu}$  for some  $\nu > 0$ , yields the result.  $\square$

### B. Proof of Theorem 2

To prove that  $I(y_0)$  is a.s. infinite, we analyze its Laplace transform  $\mathbb{E} [\exp(-sI(y_0))]$  and check if it is zero for all  $s$ . In the PPP case, the Laplace transform of the interference field is given by [11], [13]

$$\mathbb{E} [\exp(-sI(y_0))] = \exp \left( -\mathbb{E}_g \left[ \int_{\mathbb{R}^2} (1 - e^{-sg\ell(\|x-y_0\|)}) \lambda(x) dx \right] \right). \quad (32)$$

For (32) to become zero, the integral must not converge. We write

$$\int_{\mathbb{R}^2} (1 - e^{-sg\ell(\|x-y_0\|)}) \lambda(x) dx \stackrel{(a)}{\geq} \int_{\mathbb{R}^2} \frac{sg\ell(\|x-y_0\|)}{1 + sg\ell(\|x-y_0\|)} \lambda(x) dx, \quad (33)$$

where (a) follows from the inequality  $\frac{z}{1+z} \leq 1 - e^{-z}$  for  $z > -1$  [36]. Inserting the path loss function  $\ell(\|x-y_0\|) = (c + \|x-y_0\|^2)^{-1}$  into the right-hand side of (33) yields

$$2\lambda sg \int_0^\pi \int_0^\infty \frac{rF(r)}{sg + c + r^2 + y_0^2 - 2ry_0 \cos \phi} dr d\phi. \quad (34)$$

At the upper limit of the inner integral the integrand behaves as  $F(r)/r$ . So, the condition  $0 < \lim_{r \rightarrow \infty} F(r)r^\nu < \infty$ , where  $\nu \rightarrow 0$ , is sufficient for the divergence of the integral. Because the Laplace transform of  $I(y_0)$  becomes zero in this case, this concludes the proof.  $\square$

### C. Proof of Theorem 3

The proof is analogous to the proof of Theorem 1, except for the integration part. Here, the integral Identity 3 is used instead. We further exploit the fact that  $\max_r \{F(r)\} = 1$  to ensure convergence of the integrals.  $\square$



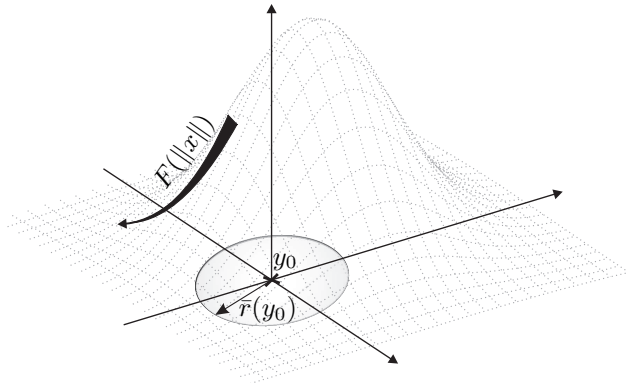


Fig. 6. Schematic illustration of the proof of Theorem 4. Shaded area around  $y_0$  represents the largest disc contained in the subharmonic region  $G$ .

#### D. Proof of Theorem 4

We follow the idea of dominant interferers which was introduced in [7] to bound the tail probability  $\mathbb{P}(I(y_0) \geq z)$ : let  $\mathcal{A}(z) \triangleq \{(x, \mathbf{g}_x) \in \Phi \times \mathbb{R}_+ : \mathbf{g}_x \ell(\|x - y_0\|) \geq z\}$  denote the set of all interferers, where each one taken by itself already results in the event  $I(y_0) \geq z$ . Clearly,

$$I(y_0) = \sum_{(x, \mathbf{g}_x) \in \mathcal{A}(z)} \mathbf{g}_x \ell(\|x - y_0\|) + \sum_{(x, \mathbf{g}_x) \in \bar{\mathcal{A}}(z)} \mathbf{g}_x \ell(\|x - y_0\|), \quad (35)$$

where the set  $\bar{\mathcal{A}}$  denotes the elements outside  $\mathcal{A}$  on the same domain, i.e.,  $\bar{\mathcal{A}}(z) \triangleq \{(x, \mathbf{g}_x) \in \Phi \times \mathbb{R}_+ : \mathbf{g}_x \ell(\|x - y_0\|) < z\}$ . Note that both sums in (35) are non-negative. Hence, we can now write

$$\begin{aligned} \mathbb{P}(I(y_0) \geq z) &\stackrel{(a)}{\geq} \mathbb{P}\left(\sum_{(x, \mathbf{g}_x) \in \mathcal{A}(z)} \mathbf{g}_x \ell(\|x - y_0\|) \geq z\right) \\ &\stackrel{(b)}{=} \mathbb{P}(|\mathcal{A}(z)| > 0) \\ &\stackrel{(c)}{=} 1 - \exp(-\Lambda(\mathcal{A}(z))), \end{aligned} \quad (36)$$

where (a) follows from removing the “non-dominant” part in (35), (b) follows from the definition of  $\mathcal{A}(z)$  and (c) is a consequence of  $|\mathcal{A}(z)|$  being Poisson distributed with mean  $\Lambda(\mathcal{A}(z))$ . Using

[11, Corollary 2.1.2],  $\Lambda(\mathcal{A}(z))$  in (36) can be computed as

$$\Lambda(\mathcal{A}(z)) = \int_{\mathbb{R}^2} \mathbb{P}(\mathbf{g} \geq z(c + \|x - y_0\|^\alpha)) \lambda(x) dx. \quad (37)$$

We now translate  $\Phi$  by the vector  $y_0$  to obtain a  $y_0$ -centric coordinate system, cf. Fig. 6. After switching to polar coordinates we obtain

$$\Lambda(\mathcal{A}(z)) = \int_0^\infty r \mathbb{P}(\mathbf{g} \geq z(c + r^\alpha)) \int_0^{2\pi} \lambda(y_0 + re^{j\phi}) d\phi dr. \quad (38)$$

We now exploit the fact that  $\lambda(x)$  is subharmonic around  $y_0$  in a region  $G$ . Let  $\bar{r}(y_0)$  denote the maximal radius for which  $b(y_0, \bar{r}(y_0))$  is contained in  $G$ . Then, (38) can be bounded as

$$\begin{aligned} \Lambda(\mathcal{A}(z)) &\stackrel{(a)}{\geq} \int_0^{\bar{r}(y_0)} r \mathbb{P}(\mathbf{g} \geq z(c + r^\alpha)) \int_0^{2\pi} \lambda(y_0 + re^{j\phi}) d\phi dr \\ &\stackrel{(b)}{\geq} 2\pi \lambda(y_0) \int_0^{\bar{r}(y_0)} r \mathbb{P}(\mathbf{g} \geq z(c + r^\alpha)) dr \\ &\stackrel{(c)}{=} 2\pi \lambda F(\|y_0\|) \int_0^{\bar{r}(y_0)} r \mathbb{P}(\mathbf{g} \geq z(c + r^\alpha)) dr, \end{aligned} \quad (39)$$

where (a) follows from limiting the upper integration limit to  $\bar{r}(y_0)$ . Inequality (b) is a consequence of subharmonicity [37, Ch.10], and (c) follows from Definition 1. Inserting (39) in (36) yields the result.  $\square$

### E. Proof of Theorem 5

We write

$$\begin{aligned} \mathcal{L}_{l(y_0)}(s) &\stackrel{(a)}{=} \mathbb{E}_\Phi \left[ \prod_{x \in \Phi} \mathbb{E}_{\mathbf{g}_x} \left[ \exp(-s \mathbf{g}_x \ell(\|x - y_0\|)) \right] \right] \\ &\stackrel{(b)}{=} \exp \left( - \int_{\mathbb{R}^2} \left( 1 - \mathcal{L}_{\mathbf{g}}(s \ell(\|x - y_0\|)) \right) \lambda(x) dx \right), \end{aligned}$$

where (a) follows from algebraic manipulations and the i.i.d. property of the  $\mathbf{g}_x$ . (b) follows from the probability generating functional and the Laplace functional of a PPP [11]. After noting that  $\mathcal{L}_{\mathbf{g}}(s) = (1 + s)^{-1}$  for exponentially distributed  $\mathbf{g}$ , the integral is computed using Identity 1 and Identity 2 for  $\alpha = 2$  and Identity 3 for  $\alpha = 4$ .

Note that (a) in the proof holds for general point processes and some approximation techniques for computing the right-hand side already exist [38]. The (b) part is for PPPs only.  $\square$

### F. Proof of Corollary 7

Solving (14) for  $\lambda$  and multiplying by  $1 - P_o(y_0)$  yields the local transmission capacity

$$c(y_0, \epsilon) = \frac{-\log(1 - \epsilon)(1 - \epsilon)}{\beta d^2 A_2(y_0, \beta d^2)} \quad (40)$$

after substituting  $P_o(y_0) \rightarrow \epsilon$ . We are interested in the case  $y_0 = o$ . Using Identity 2 (case  $T = 0$ ) we find that

$$A_2(o, \beta d^2) = -F(0) \log \beta d^2 - \int_0^\infty f(r) \log(r^2 + \beta d^2) dr. \quad (41)$$

Assuming that nodes employ pseudo-noise sequences, FH effectively thins out the point process of interferers by  $M$  (interference avoidance,  $\lambda/M$ ), while DS reduces the interference by a factor of  $M$  (interference averaging,  $\beta/M$ ), cf. [7]. Hence, using (40) and (41) the ratio  $\frac{c^{\text{FH}}(o, \epsilon)}{c^{\text{DS}}(o, \epsilon)}$  can be written as

$$\begin{aligned} \frac{c^{\text{FH}}(o, \epsilon)}{c^{\text{DS}}(o, \epsilon)} &= \frac{M}{\beta d^2 A_2(o, \beta d^2)} \frac{\beta d^2}{M} A_2(o, \frac{\beta}{M} d^2) \\ &= \frac{A_2(o, \frac{\beta}{M} d^2)}{A_2(o, \beta d^2)} \\ &\stackrel{(a)}{=} \frac{-F(0) \log \frac{\beta}{M} d^2}{A_2(o, \beta d^2)} - \frac{\int_0^\infty f(r) \log(r^2 + \frac{\beta}{M} d^2) dr}{A_2(o, \beta d^2)} \\ &\stackrel{(b)}{=} 1 + \frac{F(0) \log M}{A_2(o, \beta d^2)} + \frac{1}{A_2(o, \beta d^2)} \int_0^\infty f(r) \log \frac{r^2 + \beta d^2}{r^2 + \frac{\beta}{M} d^2} dr, \end{aligned} \quad (42)$$

where (a) follows from (14) and Remark 1 and (b) follows from algebraic manipulations. Now we show that the integral in (42) is finite. Assuming  $|f(r)| < \infty$  (which is reasonable in practical networks), we note that the integrand has no singular values. For  $M = 1$  the logarithm becomes zero and so does the integral. Since  $\log \frac{r^2 + \beta d^2}{r^2 + \frac{\beta}{M} d^2} \leq \log(1 + \frac{\beta d^2}{r^2})$  for all  $M > 0$ , we therefore

analyze the convergence of the integral

$$\left| \int_0^\infty f(r) \log\left(1 + \frac{\beta d^2}{r^2}\right) dr \right| \leq \max_r \{|f(r)|\} \int_0^\infty \log\left(1 + \frac{\beta d^2}{r^2}\right) dr < \infty. \quad (43)$$

Hence, the integral in (42) is finite.  $\square$

## REFERENCES

- [1] E. Sousa, "Performance of a spread spectrum packet radio network link in a Poisson field of interferers," *IEEE Trans. on Inf. Theory*, vol. 38, no. 6, pp. 1743–1754, Nov. 1992.
- [2] J. Ilow and D. Hatzinakos, "Analytic alpha-stable noise modeling in a Poisson field of interferers or scatterers," *IEEE Trans. on Signal Process.*, vol. 46, no. 6, pp. 1601–1611, Jun. 1998.
- [3] F. Baccelli, B. Błaszczyszyn, and P. Mühlethaler, "A spatial reuse Aloha MAC protocol for multihop wireless mobile networks," in *Proc. of Annual Conf. on Communication*, Allerton, September 2003.
- [4] F. Baccelli, B. Błaszczyszyn, and P. Mühlethaler, "An aloha protocol for multihop mobile wireless networks," *IEEE Trans. on Inf. Theory*, vol. 52, no. 2, pp. 421–436, 2006.
- [5] S. Weber, J. Andrews, and N. Jindal, "An overview of the transmission capacity of wireless networks," *IEEE Trans. on Commun.*, vol. 58, no. 12, pp. 3593–3604, Dec. 2010.
- [6] J. Andrews *et al.*, "A primer on spatial modeling and analysis in wireless networks," *IEEE Commun. Magazine*, vol. 48, no. 11, pp. 156–163, Nov. 2010.
- [7] S. Weber, X. Yang, J. Andrews, and G. de Veciana, "Transmission capacity of wireless ad hoc networks with outage constraints," *IEEE Trans. on Inf. Theory*, vol. 51, no. 12, pp. 4091–4102, Aug. 2005.
- [8] J. Andrews, S. Weber, and M. Haenggi, "Ad hoc networks: To spread or not to spread," *IEEE Commun. Magazine*, vol. 45, no. 12, pp. 84–91, Dec. 2007.
- [9] S. Weber, J. Andrews, X. Yang, and G. de Veciana, "Transmission capacity of wireless ad hoc networks with successive interference cancellation," *IEEE Trans. on Inf. Theory*, vol. 53, no. 8, pp. 2799–2814, Aug. 2007.
- [10] R. Ganti and M. Haenggi, "Interference and outage in clustered wireless ad hoc networks," *IEEE Trans. on Inf. Theory*, vol. 55, no. 9, pp. 4067–4086, Sep. 2009.
- [11] F. Baccelli and B. Błaszczyszyn, "Stochastic geometry and wireless networks, volume 1: Theory," *Foundations and Trends in Networking*, vol. 3, no. 3-4, pp. 249–449, 2009.
- [12] —, "Stochastic geometry and wireless networks, volume 2: Applications," *Foundations and Trends in Networking*, vol. 4, no. 1-2, pp. 1–312, 2009.
- [13] M. Haenggi and R. K. Ganti, "Interference in large wireless networks," *Found. Trends Netw.*, vol. 3, pp. 127–248, Feb. 2009.
- [14] R. Giacomelli, R. Ganti, and M. Haenggi, "Outage probability of general ad hoc networks in the high-reliability regime," *IEEE/ACM Trans. on Networking*, vol. 19, no. 4, pp. 1151–1163, Aug. 2011.

- [15] R. Ganti, J. Andrews, and M. Haenggi, “High-sir transmission capacity of wireless networks with general fading and node distribution,” *IEEE Trans. on Inf. Theory*, vol. 57, no. 5, pp. 3100–3116, May 2011.
- [16] S. Govindasamy and D. Bliss, “On the spectral efficiency of links with multi-antenna receivers in non-homogenous wireless networks,” in *IEEE Int. Conf. Commun. (ICC)*, Jun. 2011.
- [17] B. Błaszczyszyn and M. Karray, “Linear-regression estimation of the propagation-loss parameters using mobiles’ measurements in wireless cellular network,” in *Proc. of IEEE WiOpt*, Paderborn, 2012.
- [18] A. Hunter, R. Ganti, and J. Andrews, “Transmission capacity of multi-antenna ad hoc networks with csma,” in *Forty Fourth Asilomar Conf. on Signals, Systems and Computers (ASILOMAR)*, Nov. 2010.
- [19] R. Tanbourgi, J. Elsner, H. Jäkel, and F. Jondral, “Adaptive frequency hopping in ad hoc networks with Rayleigh fading and imperfect sensing,” *IEEE Wireless Commun. Lett.*, Jun. 2012.
- [20] —, “Lower bounds on the success probability for ad hoc networks with local FDMA scheduling,” in *Workshop on Spatial Stochastic Models for Wireless Networks (SpaSWiN)*, May 2011.
- [21] I. Akyildiz, W. Su, Y. Sankarasubramaniam, and E. Cayirci, “A survey on sensor networks,” *IEEE Commun. Magazine*, pp. 102–114, Aug. 2002.
- [22] L. Feeney, B. Ahlgren, and A. Westerlund, “Spontaneous networking: an application oriented approach to ad hoc networking,” *IEEE Commun. Magazine*, vol. 39, no. 6, pp. 176–181, Jun. 2001.
- [23] D. Brehm, “Museum exhibit shows this wireless campus never sleeps,” MIT Tech talk, December 2005, available online at: <http://web.mit.edu/newsoffice/2005/ispots.html>.
- [24] “Understanding today’s smartphone user: Demystifying data usage trends on cellular & wi-fi networks,” Mobidia, Informa Telcoms & Media, white paper, 2012.
- [25] “Dealing with density: The move to small-cell architectures,” Ruckus Wireless, white paper, 2012.
- [26] D. Avidor and S. Mukherjee, “Hidden issues in the simulation of fixed wireless systems,” *Wirel. Netw.*, vol. 7, no. 2, pp. 187–200, Mar. 2001. [Online]. Available: <http://dx.doi.org/10.1023/A:1016641723805>
- [27] R. Tanbourgi, H. Jäkel, L. Chaichenets, and F. Jondral, “Interference and throughput in aloha-based ad hoc networks with isotropic node distribution,” in *IEEE Int. Symposium on Inf. Theory (ISIT)*, Jul. 2012, pp. 616–620.
- [28] D. Stoyan, W. Kendall, and J. Mecke, *Stochastic geometry and its applications*, 2nd ed. Wiley, 1995.
- [29] J. Andrews *et al.*, “Femtocells: Past, present, and future,” *IEEE J. Sel. Areas Commun.*, vol. 30, no. 3, pp. 497–508, Apr. 2012.
- [30] M. Haenggi, *Stochastic Geometry for Wireless Networks*. Cambridge University Press, 2012.
- [31] A. Gut, *Probability: a graduate course*, ser. Springer Texts in Statistics. New York, NY: Springer, 2005.
- [32] S. G. Krantz, *Function theory of several complex variables*, 2nd ed., ser. the Wadsworth & Brooks/Cole mathematics series. Pacific Grove, Calif.: Wadsworth & Brooks, 1992.
- [33] D. Tse and P. Viswanath, *Fundamentals of wireless communication*. New York, NY, USA: Cambridge University Press, 2005.
- [34] M. Feuerstein, K. Blackard, T. Rappaport, S. Seidel, and H. Xia, “Path loss, delay spread, and outage models as functions of antenna height for microcellular system design,” *IEEE Trans. on Veh. Technol.*, vol. 43, no. 3, pp. 487–498, Aug. 1994.

- [35] I. S. Gradshteyn and I. M. Ryzhik, *Table of integrals, series, and products*, 7th ed. Elsevier/Academic Press, Amsterdam, 2007.
- [36] F. W. Olver, D. W. Lozier, R. F. Boisvert, and C. W. Clark, *NIST Handbook of Mathematical Functions*, 1st ed. New York, NY, USA: Cambridge University Press, 2010.
- [37] J. B. Conway, *Functions of one complex variable*, 2nd ed., ser. Graduate texts in mathematics ; 11. Heidelberg: Springer, 1986, vol. 2, with 30 ill.
- [38] R. Ganti and J. Andrews, "A new method for computing the transmission capacity of non-Poisson wireless networks," in *IEEE Int. Symposium on Inf. Theory (ISIT)*, Jul. 2010.